Available online at www.sciencedirect.com
ScienceDirect
Journal of Catalysis 255 (2008) 59–67
JOURNAL OF CATALYSIS
www.elsevier.com/locate/jcat

The effect of postnitridation annealing on the surface property and photocatalytic performance of N-doped TiO_2 under visible light irradiation

Xiufang Chen, Xinchen Wang *, Yidong Hou, Jianhui Huang, Ling Wu, Xianzhi Fu *

Research Institute of Photocatalysis, State Key Laboratory Breeding Base of Photocatalysis, Fuzhou University, Fuzhou 350002, China

Received 29 October 2007; revised 29 December 2007; accepted 22 January 2008

Abstract

Postnitridation annealing has a remarkable effect on the surface property and photocatalytic performance of N-doped TiO_2 for photocatalytic oxidation of ethylene. The activity of N-doped TiO_2 under visible light illumination ($\lambda > 420$ nm) can be enhanced fourfold by annealing the sample at 400 °C. Characterization results show that the thermal annealing reduces surface oxygen vacancies, removes surface-adsorbed NH_3, and facilitates the adsorption of molecular oxygen on catalyst surface. Such a surface reconstruction contributes to the enhanced photocatalytic activity of the N-doped TiO_2. The postcalcination also improves the photocatalytic stability of the N-doped TiO_2 by stabilizing nitrogen atoms in the TiO_2 lattice. A N-doped TiO_2 sample without postcalcination suffers from a gradual deactivation, due mainly to the passivation of the catalyst surface by oxidized nitrogen species (e.g., hyponitrite, nitrite ions, and nitrate ions) formed during the photocatalytic degradation of ethylene.

Keywords: Photocatalysis; Visible light; Calcination; Nitrogen; Titania

1. Introduction

Semiconductor-mediated photocatalysis has been studied widely because of its potential applications in solar energy conversion [1,2] and environmental purification [3,4]. Much effort has been devoted to the development of photocatalysts capable of using visible light, which accounts for about 43% of the incoming solar energy [5–8]. One of the main approaches to developing visible-light photocatalysts is to dope foreign atoms into ultraviolet-active catalysts like TiO_2, to extend their optical absorption to visible light. Various TiO_2-based materials have been developed on the basis of this strategy. In earlier researches, many metal ions, including transitional metal, rare earth metal, and noble metal ions, have been used to modify the optical and photocatalytic properties of TiO_2. Some metal ions (V^{5+}, Cr^{3+}, Fe^{3+}, Mo^{5+}, Ru^{3+}, Rh^{3+}) have been reported to extend the photoactive region of TiO_2 to visible light [5,9,10], but there remains great concern about introducing recombination centers of charge carriers in some cases. Recently, it was reported that doping of such anion elements as nitrogen, carbon, and sulfur into TiO_2 leads to a shift in the onset of absorption of TiO_2 to visible light and thus increases its overall photocatalytic efficiency [6,11,12]. Since these reports appeared, much attention has been given to investigating the nature of nitrogen atoms doped in TiO_2 and improving the activity of N-doped TiO_2 under visible light irradiation [13]. In various environmental and synthetic applications of N-doped TiO_2 catalysts, their photostability or instability remains an important issue [14].

N-doped TiO_2 catalysts are synthesized conventionally by heating TiO_2 with NH_3 gas at high temperatures. An inherent disadvantage to N-doped TiO_2 thus prepared is the formation of numerous defect states, including oxygen vacancies, due to the use of rather reductive NH_3 gas [15,16]. Photoexcited charge carriers are susceptible to recombination at surface defect sites, leading to low photocatalytic activity. The low photocatalytic activity also can be due to coverage of the catalyst surface by NH_3 molecules.

In attempts to improve the photocatalytic performance of N-doped TiO_2 catalysts, various physicochemical methods have been applied to modify N-doped TiO_2 photocatalysts. For example, Gao et al. [17] incorporated WO_3 into $TiO_{2-x}N_x$ by a

* Corresponding authors. Fax: +86 591 83738608.
E-mail addresses: xcwang@fzu.edu.cn (X. Wang), xzfu@fzu.edu.cn (X. Fu).

0021-9517/$ – see front matter
doi:10.1016/j.jcat.2008.01.025

wet impregnation method and found that the $WO_3/TiO_{2-x}N_x$ exhibited higher photocatalytic activity than both TiO_2 and N-doped TiO_2. Another study found that ZrO_2-modified mesoporous $TiO_{2-x}N_x$ exhibited enhanced photocatalytic activity for the decomposition of ethylene under visible light [18]. Morikawa et al. [19] used various metal ions, including Cu^{2+}, Pt^{6+}, Ni^{2+}, Zn^{2+} and La^{3+}, to modify $TiO_{2-x}N_x$ and found that the photocatalytic activity of the $TiO_{2-x}N_x$ was enhanced by modification with Cu^{2+} and Pt^{6+}. Li et al. [20] reported that the photocatalytic activity of N-F-co-doped TiO_2 was superior to that of pure TiO_2 under both ultraviolet and visible light irradiations.

In this paper, we report an effective method to improve the photocatalytic activity and stability of N-doped TiO_2 catalysts by a simple postnitridation annealing treatment, which has been used widely to adjust the optical properties of III–V nitride semiconductors, such as GaN [21,22]. We investigated the effects of postsintering on textural, optical, and surface properties, as well as photocatalytic activity of N-doped TiO_2. We also evaluated the photocatalytic stability of N-doped TiO_2. We chose visible-light-induced mineralization of ethylene to CO_2 as the model reaction to evaluate the photocatalytic performance of N-doped TiO_2.

2. Experimental

2.1. Catalyst preparation

An amorphous TiO_2 xeogel was prepared by a sol–gel method as described previously [23]. The as-prepared TiO_2 xeogel was then heated under flowing NH_3 gas (flow rate: 400 mL min^{-1}) at 400 °C for 3 h, followed by naturally cooling to room temperature under NH_3. This yielded a pale-yellow solid, which was then annealed at 200–600 °C for 2 h in static air to produce final N-doped TiO_2 samples. The N-doped TiO_2 catalysts annealed at temperatures of 200, 300, 400, 500, and 600 °C were designated NT200, NT300, NT400, NT500, and NT600, respectively. The sample prepared without postcalcination was designated NT and used as a reference.

2.2. Characterization

X-ray diffraction (XRD) measurements were performed on a Bruker D8 Advance X-ray diffractometer with Cu$K\alpha_1$ radiation ($\lambda = 1.5406$ Å). A Varian Cary 500 Scan UV–visible system equipped with a Labsphere diffuse reflectance accessory was used to obtain the light absorption spectra of catalysts. Nitrogen adsorption–desorption isotherms were collected at 77 K using a Micromeritics ASAP 2010 instrument. Photoluminescence (PL) spectra were obtained at 77 K on an Edinburgh Analytical Instruments FL/FSTCSPC920. The electron spin resonance (ESR) spectra were obtained in air ambience at 100 K without illumination using a Bruker EMX-10/12 ESR spectrometer operated at the X-band 9.5 GHz. X-ray photoelectron spectra (XPS) were recorded on a VG ESCALB MK-II XPS System with a monochromatized Mg$K\alpha$ X-ray source (35 W). All binding energies were referenced to the C_{1s} peak at 284.6 eV of surface adventitious carbon. Temperature-programmed desorption (TPD) experiments were conducted using an AutoChem II 2920 TPD instrument. Samples were evacuated at 100 °C for 3 h, followed by cooling to 40 °C under flowing He gas (30 mL min^{-1}) for 30 min. Subsequently, the temperature of catalyst bed was increased gradually to 600 °C at a rate of 5 °C min^{-1} using He as a carrier gas (flow rate: 10 mL min^{-1}). The main desorbed species were detected by quadruple mass analysis (QMA), scanning the m/e values of 12, 14, 16, 17, 18, 28, 30, 44, and 46. Here $m/e = 17$ instead of $m/e = 16$ was chosen for determining ammonia, because of the possible appearance of oxygenated molecules, which can participate in $m/e = 16$ fragmentation. Note that the signal at $m/e = 17$ also includes water fragmentation participation; however, it is possible to calculate the relative abundance of $m/e = 17$ due solely to ammonia, because the relative water fragmentation ratio of abundance $m/e = 17$/abundance $m/e = 18$ is given by the constructor as 23.00%. Fourier transformed infrared (FTIR) spectra were recorded using a Nicolet Magna 670 FTIR spectrometer. The samples were mixed with KBr at a concentration of ca. 10%.

2.3. Photocatalytic activity measurements

Photocatalytic reactions were carried out in a fixed-bed reactor (35 × 28 × 1 mm) operated in a single-pass mode. A 500 W Xe-arc lamp with a 420-nm cutoff filter was used as the visible light source. The weight of catalyst (50–70 mesh) was kept at 1.1 g. Ethylene diluted in water-saturated zero air (79% nitrogen, 21% oxygen; total hydrocarbons <1 ppm) was used to afford a reactant stream. The flow rate of reactant stream was maintained at 20 mL min^{-1}. The initial concentrations of ethylene and carbon dioxide in the stream were 705 and 0 ppm, respectively. The analysis of CO_2 was performed with an online gas chromatograph (HP6890) equipped with a thermal conductivity detector and a Porapak R column. The temperature of the reactor under illumination was 30 °C, as measured by using a J-type thermocouple. Ethylene was found to be stable in the catalyst-loaded reactor without visible light illumination. No degradation of ethylene was observed when it was illuminated in the absence of catalyst.

3. Results

3.1. Effects of postsintering on textural and optical properties

Fig. 1 shows the XRD patterns of N-doped TiO_2 samples annealed at different temperatures. No remarkable change in the patterns can be seen for the samples sintered below 400 °C. The crystalline phase of these samples was anatase. A rutile phase appeared when the N-doped TiO_2 was annealed at temperatures above 400 °C. The phase transformation from anatase to rutile was completed at 600 °C. The crystal sizes of TiO_2 in N-doped TiO_2 annealed at different temperatures are given in Table 1. When N-doped TiO_2 was annealed at 400 °C, the crystal size of anatase increased slightly, from 6.8 to 9.0 nm. As the temperature increased to 500 °C, the crystal size of anatase increased

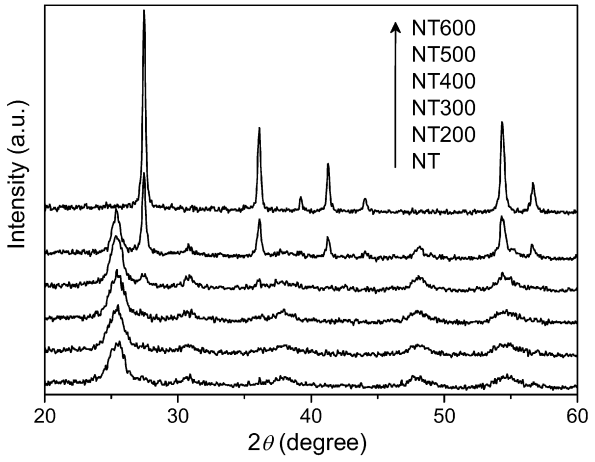

Fig. 1. XRD patterns of N-doped TiO_2 catalysts annealed at different temperatures.

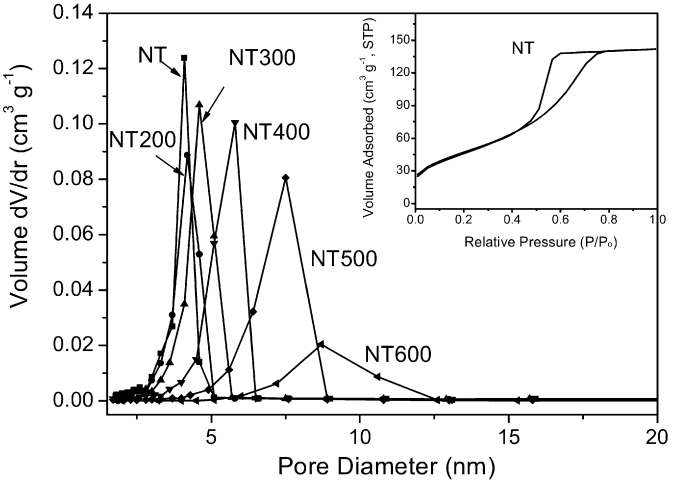

Fig. 2. BJH pore-size distribution curves of N-doped TiO_2 catalysts annealed at different temperatures and the corresponding isotherm of NT as the inset. The pore-size distribution was determined from the desorption branch of the isotherms.

noticeably, to 15.5 nm, due to the agglomeration of particles during the high-temperature sintering. In addition, the crystal size of rutile increased dramatically when the sample was heated at temperatures above 400 °C. These results demonstrate that postsintering below 400 °C had only a slight influence on the phase structure and crystal size of the sample, but higher annealing temperatures (>400 °C) induced crystal growth and phase transformation from anatase to rutile, considered the less active phase of TiO_2 for photocatalytic degradation of organic compounds [24,25].

Fig. 2 shows the pore size distributions of N-doped TiO_2 sintered at different temperatures. The inset shows the typical nitrogen isotherm of NT. The isotherm exhibits stepwise adsorption and desorption, indicative of three-dimensional intersection of a solid porous structure [26]. The results of nitrogen sorption, summarized in Table 1, show that postsintering treatment reduced the specific surface area of N-doped TiO_2. The sample without postcalcination was a mesoporous material with a high specific surface area of 172 $m^2\,g^{-1}$, which decreased to 115 $m^2\,g^{-1}$ after annealing at 400 °C. The sample sintered at 600 °C exhibited a decrease in surface area to 13 $m^2\,g^{-1}$, along with a decrease in total pore volume to 0.05 $cm^3\,g^{-1}$, due to excessive growth of TiO_2 crystals, as well as partial collapse of the mesoporous framework.

Fig. 3 shows the light absorption properties of N-doped TiO_2 samples annealed at different temperatures. All of the N-doped TiO_2 samples demonstrated significant absorption in the visible light region between 400 and 550 nm, which is a typical absorption region for nitrogen-doped TiO_2 materials. When postsintering temperature was below 400 °C, no significant alteration in the visible-light absorption of N-doped TiO_2 samples occurred. But for samples annealed at temperatures above 400 °C, absorption in the visible light region decreased with increasing temperatures. This decreased absorption indicates a loss of nitrogen atoms in TiO_2, because nitrogen atoms are easily replaced by oxygen atoms during thermal annealing at high temperatures, as confirmed by the XPS results (Table 1). Note that the absorption edge of the N-doped TiO_2 samples demonstrated a gradual red-shift with increasing temperature from 400 °C to 600 °C. This is attributed to the increased amount of rutile in N-doped TiO_2 sintered at temperatures above 400 °C (see Ta-

Table 1
Textural properties and surface chemical composition of N-doped TiO_2 annealed at different temperatures

Sample	Crystal phase	Crystal size[a] (nm)	S_{BET}[b] ($m^2\,g^{-1}$)	V[c] ($cm^3\,g^{-1}$)	D_{BJH}[d] (nm)	Surface N/Ti[e] (at%)
NT	Anatase	6.8	172	0.22	5.1	1.65
NT200	Anatase	7.0	165	0.22	5.3	1.01
NT300	Anatase	7.3	166	0.25	6.0	0.88
NT400	Anatase (87%) Rutile (13%)	Anatase (9.0) Rutile (7.5)	115	0.20	7.0	0.83
NT500	Anatase (39%) Rutile (61%)	Anatase (15.5) Rutile (28.7)	64	0.16	9.8	0.82
NT600	Rutile	36.2	13	0.05	13.6	0.47

[a] Calculated by applying the Scherrer formula on the anatase (101) or rutile (110) diffraction peak.
[b] BET surface area calculated from the linear part of the BET plot ($P/P_0 = 0.1$–0.2).
[c] Total pore volume, taken from the volume of N_2 adsorbed at $P/P_0 = 0.991$.
[d] Average pore diameter, estimated using the desorption branch of the isotherm and the Barrett–Joyner–Halenda (BJH) formula.
[e] Calculated from the results of XPS spectra for the N_{1s} region.

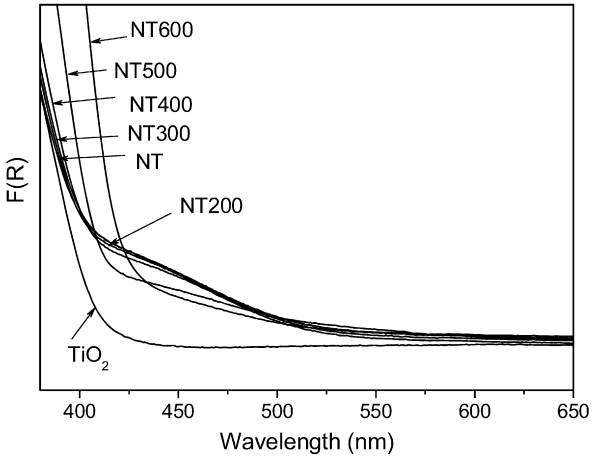

Fig. 3. UV–visible absorption spectra of the N-doped TiO_2 catalysts annealed at different temperatures.

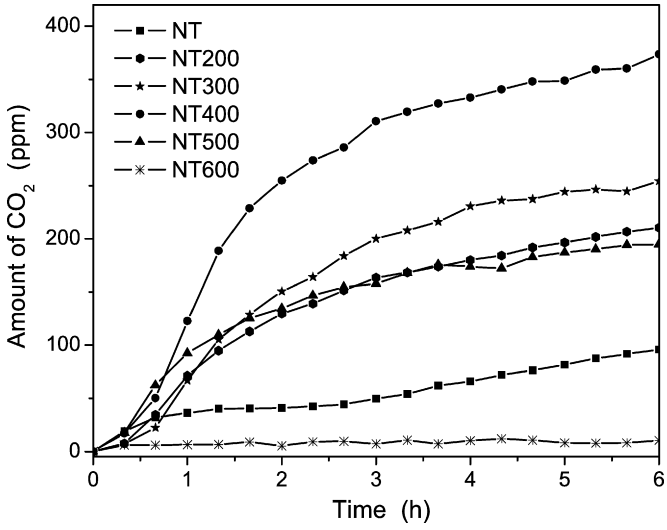

Fig. 4. The amount of CO_2 produced from the photocatalytic degradation of ethylene on N-doped TiO_2 annealed at different temperatures.

ble 1), because rutile has a lower band-gap energy than anatase (3.0 eV vs. 3.2 eV).

3.2. *Effects of postsintering on photocatalytic activity and stability*

Photocatalytic activity of N-doped TiO_2 samples for decomposing ethylene under visible light ($\lambda > 420$ nm) was found to be dependent on postcalcination temperature. Fig. 4 shows visible-light-induced photocatalytic activity of N-doped TiO_2 sintered at different temperatures. The activity increased rapidly with increasing postcalcination temperature up to 400 °C. After reaction for 6 h, NT400 showed the highest CO_2 evolution of 373 ppm, about 4 times higher than that of NT (96 ppm). The activity for NT500 and NT600 dropped abruptly, however. Note that thermal annealing of N-doped TiO_2 at temperatures above 400 °C caused the phase transformation from anatase to rutile and loss of surface area of the sample; as a result, NT500 and NT600 had lower photocatalytic activity than NT400. In the

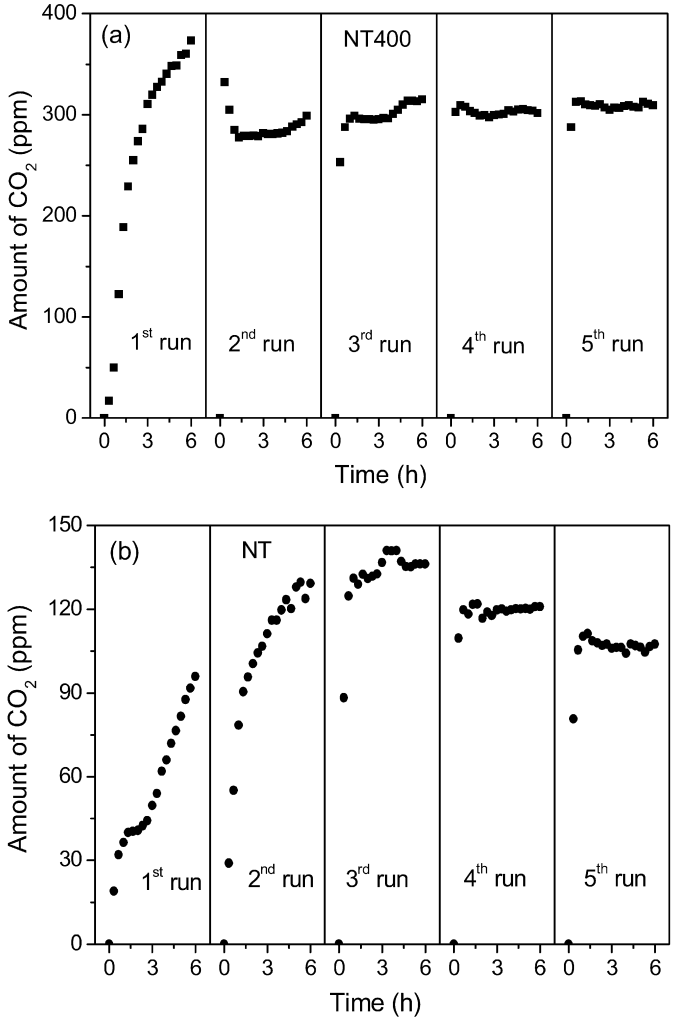

Fig. 5. Cycling runs for the photooxidation of ethylene on NT400 (a) and NT (b).

range of 200–400 °C, although postannealing induced a small increase in crystal size and a slight decrease in surface area, the sample still exhibited enhanced activity with increasing temperature. This indicates that other factors (e.g., changes in surface properties) might favorably influence the photocatalytic performance of N-doped TiO_2 with postannealing treatment.

We also evaluated the photocatalytic stability of NT and NT400; the results are shown in Fig. 5. The amount of CO_2 increased with irradiation time in the first run for NT400 (see Fig. 5a). Although deactivation occurred in the initial stage of the second run, the concentration of CO_2 in the stream remained at a relatively steady state of ca. 300 ppm during the last three runs. The evolution rate of CO_2 over 18 h of visible-light irradiation in the last three runs reached 14.5 $\mu mol\,h^{-1}$. For NT (see Fig. 5b), the amount of CO_2 increased gradually in the first two runs. In the third run, it reached a maximum of 130 ppm and then began to decrease. In the last two runs, it decreased even further. The average evolution rate of CO_2 in the last three runs was calculated to be 5.7 $\mu mol\,h^{-1}$ for NT. Clearly, both the activity and stability of N-doped TiO_2 photocatalyst were enhanced by the postannealing treatment.

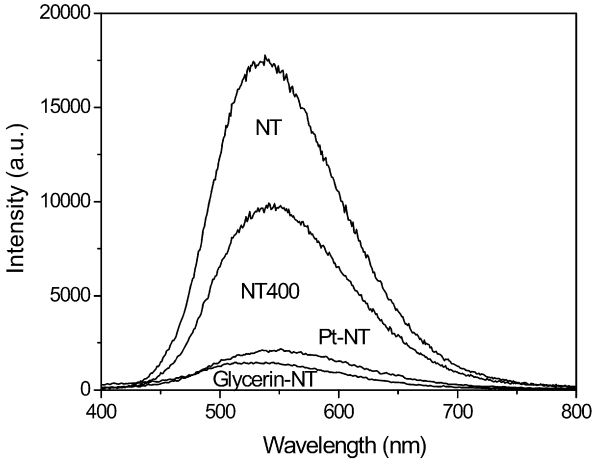

Fig. 6. PL spectra of NT, NT400, Pt-NT and glycerin-NT. The samples were excited at 325 nm under vacuum at 77 K.

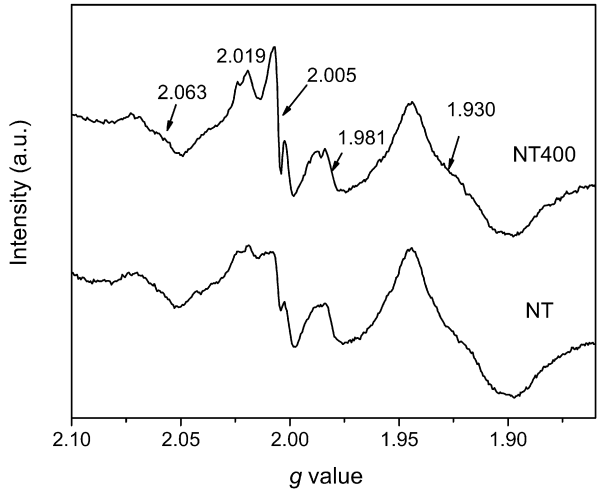

Fig. 7. ESR spectra of NT and NT400 measured at 100 K without irradiation.

3.3. Effects of postsintering on surface properties

The PL process is closely related to surface states and stoichiometric chemistry, which generally would be altered by an annealing process [27]. Fig. 6 shows the PL spectra of NT and NT400. A broad visible PL band centered at 540 nm can be seen for both NT and NT400. There may be multifold PL processes contributing to the broad nature of the visible PL band. According to the literature [28,29], the visible PL band is related to shallow traps associated with oxygen vacancies. It is known that in anatase TiO_2, the oxygen vacancy states are below the lower end of the conduction band at 0–1 eV [29]. Oxygen vacancies can form both in the bulk and on the surface of TiO_2.

To study the nature of the PL process in depth, we used Pt and glycerin as scavengers for electrons and holes photogenerated on N-doped TiO_2, respectively. The results, shown in Fig. 6, demonstrate that the visible PL band was obviously quenched in the presence of Pt or glycerin. Because PL is sensitive to the sample environment, this result suggests that the visible PL was a surface phenomenon. Moreover, postsintering at 400 °C for NT led to significant quenching of PL. The lower intensity of the visible PL band suggests that the postsintering resulted in a decrease in the recombination of electron–hole pairs. Because the broad visible band is associated with electrons trapped at surface defect sites, the quenching of PL of NT400 indicates a decrease in the number of surface defects. This is consistent with previous results indicating that postsintered treatment can remove surface defects [21,22]. Zhang et al. [30] also reported that the visible PL of TiO_2 film is strongly diminished after sintering, suggesting the removal of defects associated with oxygen vacancies. Consequently, reduction of oxygen vacancies is considered an important contributing factor to the enhanced photocatalytic activity of N-doped TiO_2 catalysts. This is consistent with recent results of Miyauchi et al. [31].

Fig. 7 gives the ESR spectra measured at 100 K without illumination for NT and NT400. The signals at $g = 2.005$, 2.019, and 2.063 can be assigned to O_2^- adsorbed on the catalyst surface, as confirmed previously by Carter et al. [32,33]. The greater intensity of the O_2^- signals of NT400 compared with those of NT suggests a greater amount of surface-adsorbed oxygen on NT400 than on NT. The signals at $g = 1.930$ and 1.981 for N-doped TiO_2 can be attributed to Ti^{3+} on the surfaces [32, 34,35]. Closer inspection of the ESR spectra reveals lower intensity of the Ti^{3+} signals of NT400 compared with those of NT, probably due to the presence of more molecular oxygen on NT400 than on NT. Oxygen molecules adsorbed on the surface of catalysts are known to be effective trapping sites for photogenerated electrons [3,25] and act as a reactant for the oxidative decomposition of organic compounds. Therefore, the presence of a high amount of molecular oxygen on the catalyst surface facilitates photocatalysis.

We analyzed the surface composition and electronic state of N-doped TiO_2 by XPS. Figs. 8a and 8b show the XPS spectra of N_{1s} of N-doped TiO_2 samples before and after the photocatalytic reaction. All of the N-doped TiO_2 samples exhibited a broad peak that can be fitted by three peaks at 396.0, 399.6, and 401.6 eV. The strongest peak at 399.6 eV can be assigned to nitrogen atoms in the environment of O–Ti–N linkages [18, 36,37], as also supported by the low $Ti_{2p3/2}$ binding energy of N-doped TiO_2 compared with pure TiO_2. The peaks at 396.0 and 401.6 eV can be attributed to Ti–N bonds [6] and nitrogen species bound to various surface oxygen sites (NO-like species) [18,38,39], respectively. The XPS spectra of NT (Fig. 8a) shows that the peak intensities at 399.6 and 396.0 eV decreased after the reaction, due mainly to removal of the nitrogen atoms from TiO_2 matrix. Note that the peak intensity at 401.6 eV increased after the reaction; this implies partial conversion of nitrogen atoms in TiO_2 to oxidized nitrogen species during the course of the reaction. Fig. 8b shows the XPS spectra of NT400 before and after the reaction. Like NT, the peak at 396.0 eV also decreased in intensity after the reaction; however, there was no significant change in the peak intensities at 401.6 and 399.6 eV, indicating that the lattice-nitrogen atoms in NT400 remained relatively stable under visible light irradiation. This finding is supported by the XPS analysis. As shown in Fig. 8c, the binding energy of $Ti_{2p3/2}$ for the used NT sample increased by 0.2 eV compared with the fresh sample. The shift may be

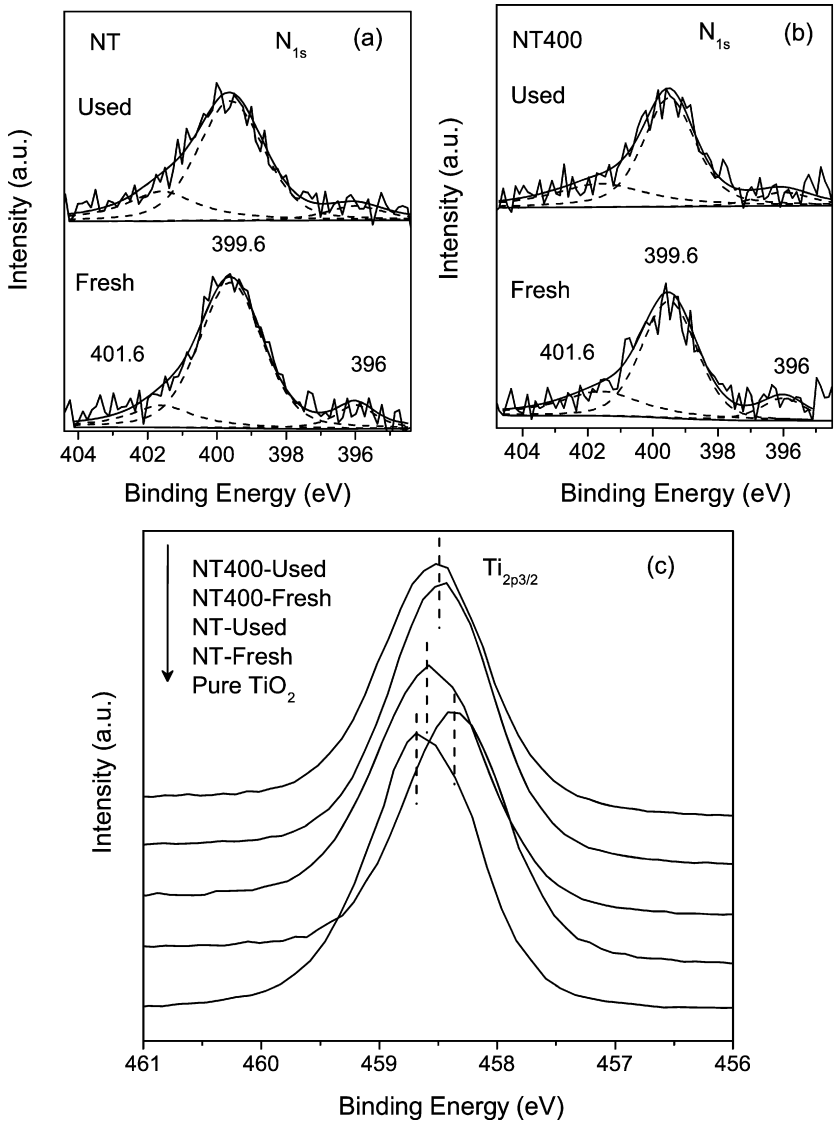

Fig. 8. XPS spectra of N_{1s} (a, b), and $Ti_{2p3/2}$ (c) for NT and NT400 before and after reaction.

due to the replacement of nitrogen in O–Ti–N by oxygen with higher electronegativity, which changes the electronic density around the Ti atom. But no dramatic shift in binding energy of $Ti_{2p3/2}$ occurred for the used NT400, demonstrating the advantage of postsintering in stabilizing nitrogen in TiO_2.

Fig. 9 shows the TPD-MS spectra of NT and NT400 heated under pure He flow. Obviously, NH_3 ($m/e = 17$), NO ($m/e = 30$), and N_2 ($m/e = 28$) desorbed from the N-doped TiO_2 samples during TPD. The $m/e = 30$ and 28 are mostly associated with NO and N_2 desorption. CO was excluded, because no $m/e = 12$ was detected under the instrument's resolution. We also assume that no NO_2 was desorbed from both NT and NT400, because no $m/e = 46$ was found in the total mass spectrum. Fig. 9a shows the thermal desorption spectra of NH_3. The evolution of NH_3 was evaluated based on the profile of $m/e = 17$ (ammonia + water), from which the participation of $m/e = 18$ (only water) was subtracted, as explained in Section 2. As shown in Fig. 9a, clearly much less NH_3 was desorbed from NT400 than from NT. This demonstrates that the as-prepared N-doped TiO_2 (NT) adsorbed a large amount of NH_3 and that postsintering treatment removed the NH_3. This finding is in agreement with FTIR analyses. Fig. 9b shows the thermal desorption spectra of NO for NT and NT400. The broad desorption band peaking at 370 °C can be seen only for NT. Fig. 9c shows the thermal desorption spectra N_2 for NT and NT400. Two N_2 desorption peaks at 170 and 525 °C can be seen for NT; for NT400, however, these peaks shift toward higher temperatures, 270 and 550 °C. These results confirm that nitrogen atoms doped in NT400 are more stable than those in NT.

Fig. 10a displays FTIR spectra of NT before and after the reaction. All of the samples displayed strong bands at 3400 and 1620 cm^{-1}, corresponding to surface hydroxyl groups and adsorbed water molecules [40,41]. For the fresh NT, two additional bands at 1400 and 1385 cm^{-1} can be seen; the former is attributed to adsorbed-NH_3 molecules [42], whereas the later is due to the formation of hyponitrite [17,43]. After the reaction, the NH_3 band decreased and the hyponitrite band increased. In addition, two new weak bands at 1554 and 1350 cm^{-1} ap-

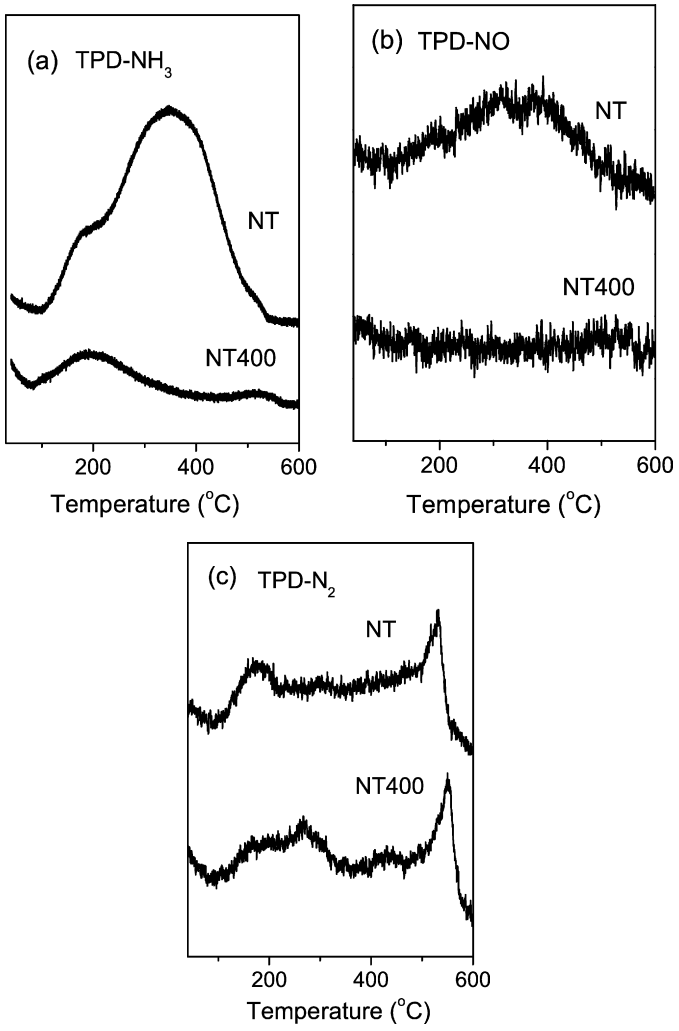

Fig. 9. TPD-MS spectra of NH_3 (a), NO (b) and N_2 (c) for NT and NT400.

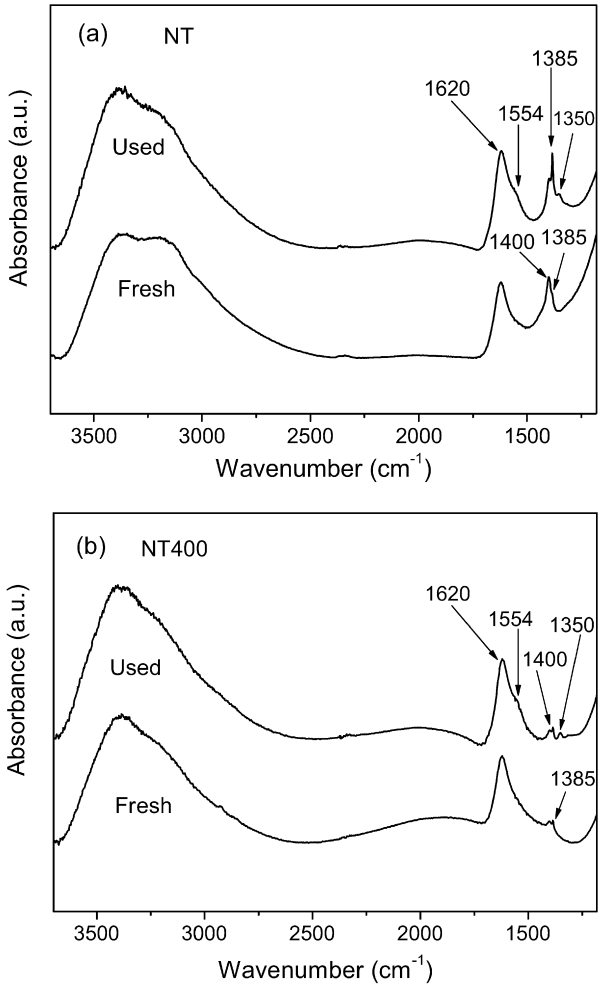

Fig. 10. FTIR spectra of NT (a) and NT400 (b) before and after reaction.

peared. The new bands can be ascribed to NO-like species such as nitrite ions or nitrate ions [43,44]. These results indicate that adsorbed-NH_3 molecules were partially desorbed or converted into NO-like species during the course of the reaction. In Fig. 10b, for the fresh NT400, the band at 1400 cm^{-1}, corresponding to NH_3, was dramatically decreased in intensity compared with the fresh NT. This suggests that NH_3 molecules adsorbed on the surface hydroxyl groups of the sample were mostly removed by the postsintering treatment at 400 °C. Note that absorption band for NO-like species also was observed for the used NT400, but this band was of much weaker intensity than that of the used NT.

4. Discussion

Surface hydroxyl groups are known to play an important role in photocatalysis; they react with photogenerated holes, producing active hydroxyl radicals [45]. In addition, surface hydroxyl groups can act as surface sites for adsorbing organic molecules, which also efficiently capture photogenerated holes [3]. The trapping of holes stabilizes photogenerated electron–hole pairs, improving photocatalytic efficiency. In the NT, NH_3 readily adsorbed on the catalyst surface during the nitridation process, due to the numerous acidic hydroxyl groups on the NT surface (see the results of the FTIR analysis). The presence of these surface-adsorbed NH_3 decreased the number of surface sites accessible for reactants, resulting in low photocatalytic activity. This is believed to be one of the main mechanisms accounting for the low activity of NT. In contrast, in NT400, most of the NH_3 was removed during thermal annealing, as confirmed by TPD-MS and FTIR spectra (Figs. 9a and 10). Consequently, NT400 had a high density of surface hydroxyl groups for adsorbing organic substrates as well as capturing photogenerated holes, thereby stabilizing the charge carriers of the sample. Thus, the activity of N-doped TiO_2 was enhanced by the postsintering treatment.

We conducted an additional experiment to confirm the detrimental effect of NH_3. In this experiment, NT was washed with pure water several times to remove adsorbed NH_3, as confirmed by IR spectra (not shown). The resultant sample was designated NT-cleaning. Fig. 11 displays the photocatalytic activity of NT, NT-cleaning, and NT400. The production of CO_2 from NT was markedly improved after the cleaning treatment; however, NT-cleaning still had much lower photocatalytic activity than NT400. This implies that the enhanced photocatalytic ac-

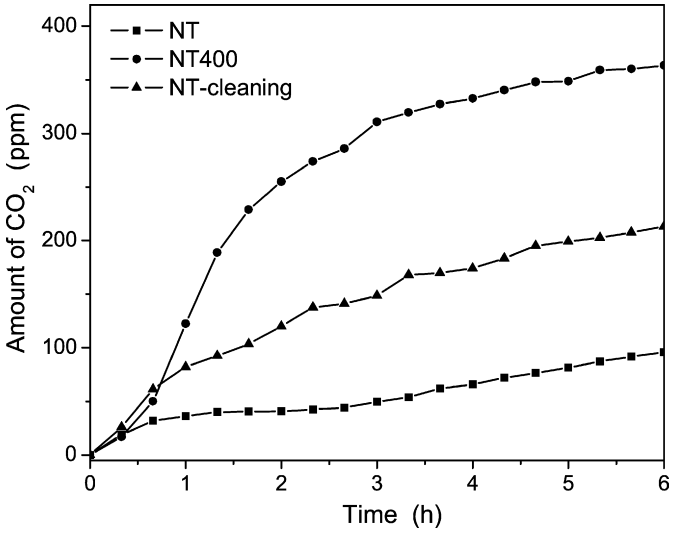

Fig. 11. The amount of CO_2 produced from the photocatalytic degradation of ethylene on NT, NT-cleaning and NT400.

tivity is also related to other factors, such as the reduction of surface defect sites.

Deactivation of a photocatalyst has been ascribed to the accumulation of less reactive species on the catalyst surface [46]. Our XPS and FTIR results demonstrate that the activity of N-doped TiO_2 decreased with an increase in the amount of oxidized nitrogen species such as hyponitrite, nitrite ions, or nitrate ion. The oxidized nitrogen species formed in the ethylene photooxidation can cover surface active sites of the catalyst, as indeed was confirmed by the FTIR analysis. Moreover, the oxidation of nitrogen species consumes photogenerated holes, inhibiting the production of reactive hydroxyl radicals, leading to a gradual deactivation of N-doped TiO_2. As shown in Fig. 5a, the gradual increase in the activity for NT400 in the first run can be attributed to the gradual removal of adsorbed-NH_3 during the course of the reaction. Simultaneously, some adsorbed-NH_3 was converted to oxidized nitrogen species, covering surface active sites of the sample. This caused a slight deactivation in the initial stage of the second run. Because only a small amount of NH_3 was adsorbed on the catalyst surface, the process was quick, with only a small amount of oxidized nitrogen species formed (see the FTIR spectra in Fig. 10b); thus, the activity remained steady during the last three runs. But for NT, a large amount of NH_3 was adsorbed on its surface (see the FTIR analysis in Fig. 10a), poisoning most of surface sites; thus, the activity of NT was much lower than that of NT400. As the reaction progressed, NH_3 was gradually removed from the surface, leading to enhanced activity for the first and second runs; however, the NH_3 molecules also were converted to the oxidized nitrogen species, which act as poisoning species for the reaction. The removal of NH_3 and the production of oxidized nitrogen species compete for the catalyst surface as the reaction progressed; consequently, the activity increased slightly in the third run and reached a steady state thereafter. With the gradual oxidation of NH_3, the amount of oxidized nitrogen species on the surface of catalyst increased, resulting in deactivation in the fourth and fifth runs.

The loss of nitrogen in the N-doped TiO_2 was another factor contributing to its deactivation during the photocatalytic degradation of organic compounds. XPS analyses (Fig. 8) showed that the amount of lattice-nitrogen in the N-doped TiO_2 decreased after the reaction. The loss of nitrogen was due mainly to the oxidation of lattice-nitrogen by photogenerated holes. Note that lattice-nitrogen atoms are responsible for the catalytic activity of TiO_2 in visible light [17,18,47]. Because postsintering treatment at 400 °C was favorable for stabilizing nitrogen atoms in the lattice of TiO_2, NT400 was more stable than NT for the photocatalytic oxidation of ethylene.

5. Conclusion

Our findings indicate that postirridation annealing is a simple method for improving both the activity and stability of N-doped TiO_2 catalyst for the photocatalytic oxidation of ethylene under visible light. The optimum annealing temperature was found to be 400 °C. The annealing effectively minimized surface defects, facilitated the adsorption of oxygen molecules, and removed adsorbed NH_3 on the catalyst surface. This sintering-induced surface reconstruction explains the enhanced photocatalytic performance of N-doped TiO_2. The deactivation of N-doped TiO_2 sample was prevented by annealing the sample at 400 °C, due to the stabilization of nitrogen in the TiO_2 lattice. The enhanced photocatalytic activity and prevention of catalyst deactivation will lead to more cost-effective operation and improved organic matter mineralization efficiency for practical applications.

Acknowledgments

This work was supported by the National Basic Research Program of China (973 Program, 2007CB613306), the National Natural Science Foundation of China (20537010 and 20603007), the New Century Excellent Talents in University of China (NCET-07-0192), and the Natural Science Foundation of Fujian Province of China (2006J0160). The authors thank the reviewers for their helpful suggestions and comments on the manuscript.

References

[1] M.A. Fox, M.T. Dulay, Chem. Rev. 93 (1993) 341.
[2] A. Fujishima, K. Honda, Nature 37 (1972) 238.
[3] M.R. Hoffmann, S.T. Martin, W. Choi, D.W. Bahnemannt, Chem. Rev. 95 (1995) 69.
[4] A.L. Linsebigler, G.Q. Lu, J.T. Yates, Chem. Rev. 95 (1995) 735.
[5] E. Borgarello, J. Kiwi, M. Grätzel, E. Pelizzetti, M. Visca, J. Am. Chem. Soc. 104 (1982) 2996.
[6] R. Asahi, T. Morikawa, T. Ohwaki, K. Aoki, Y. Taga, Science 293 (2001) 269.
[7] A. Kudo, K. Omori, H. Kato, J. Am. Chem. Soc. 121 (1999) 11459.
[8] H. Kato, H. Kobayashi, A. Kudo, J. Phys. Chem. B 106 (2002) 12441.
[9] W. Choi, A. Termin, M.R. Hoffmann, J. Phys. Chem. 98 (1994) 13669.
[10] J.F. Zhu, F. Chen, J.L. Zhang, H.J. Chen, M. Anpo, J. Photochem. Photobiol. A 180 (2006) 196.
[11] T. Umebayashi, T. Yamaki, H. Itoh, K. Asai, Appl. Phys. Lett. 81 (2002) 454.
[12] S. Sakthivel, H. Kisch, Angew. Chem. Int. Ed. 42 (2003) 4908.

[13] J.L. Gole, J.D. Stout, C. Burda, Y.B. Lou, X.B. Chen, J. Phys. Chem. B 108 (2004) 1230.
[14] N. Serpone, J. Phys. Chem. B 110 (2006) 24287.
[15] H. Irie, Y. Watanabe, K. Hashimoto, J. Phys. Chem. B 107 (2003) 5483.
[16] M. Batzill, E.H. Morales, U. Diebold, Phys. Rev. Lett. 96 (2006) 026103.
[17] B.F. Gao, Y. Ma, Y.A. Cao, W.S. Yang, J.N. Yao, J. Phys. Chem. B 110 (2006) 14391.
[18] X.C. Wang, J.C. Yu, Y.L. Chen, L. Wu, X.Z. Fu, Environ. Sci. Technol. 40 (2006) 2369.
[19] T. Morikawa, Y. Irokawa, T. Ohwaki, Appl. Catal. A 314 (2006) 123.
[20] D. Li, H. Haneda, S. Hishita, N. Ohashi, Chem. Mater. 17 (2005) 2596.
[21] S.O. Kucheyev, J.S. Williams, S.J. Pearton, Mater. Sci. Eng. 33 (2001) 51.
[22] H.W. Huang, C.C. Kao, J.Y. Tsai, C.C. Yu, C.F. Chu, J.Y. Lee, S.Y. Kuo, C.F. Lin, H.C. Kuo, S.C. Wang, Mater. Sci. Eng. B 107 (2004) 237.
[23] X.Z. Fu, W.A. Zeltner, Q. Yang, M.A. Anderson, J. Catal. 168 (1997) 482.
[24] A. Sclafani, J.M. Herrmann, J. Phys. Chem. 100 (1996) 13655.
[25] J.C. Yu, J. Lin, D. Lo, S.K. Lam, Langmuir 16 (2000) 7304.
[26] R.C. Nádia, F. Machado, V.S. Santana, Catal. Today 107–108 (2005) 595.
[27] J.Y. Shi, J. Chen, Z.C. Feng, T. Chen, Y.X. Lian, X.L. Wang, C. Li, J. Phys. Chem. C 111 (2007) 693.
[28] X.F. Song, L. Gao, Langmuir 23 (2007) 11850.
[29] N. Serpone, D. Lawless, R. Khairutdinov, J. Phys. Chem. 99 (1995) 16646.
[30] D. Zhang, J.A. Downing, F.J. Knorr, J.L. McHale, J. Phys. Chem. 110 (2006) 21890.
[31] M. Miyauchi, M. Takashio, H. Tobimatsu, Langmuir 20 (2004) 232.
[32] E. Carter, A.F. Carley, D.M. Murphy, J. Phys. Chem. C 111 (2007) 10630.
[33] T. Hirakawa, H. Kominami, B. Ohtani, Y. Nosaka, J. Phys. Chem. B 105 (2001) 6993.
[34] S. Joung, T. Amemiya, M. Murabayashi, K. Itoh, Appl. Catal. A 312 (2006) 20.
[35] Y. Nakaoka, Y. Nosaka, J. Photochem. Photobiol. A 110 (1997) 299.
[36] H.X. Li, J.X. Li, Y.N. Huo, J. Phys. Chem. B 110 (2006) 1559.
[37] J.W. Wang, W. Zhu, Y.Q. Zhang, S.X. Liu, J. Phys. Chem. C 111 (2007) 1010.
[38] S.H. Overbury, D.R. Mullins, D.R. Huntley, L. Kundakovic, J. Catal. 186 (1999) 296.
[39] J.A. Rodriguez, T. Jirsak, G. Liu, J. Hrbek, J. Dvorak, A. Maiti, J. Am. Chem. Soc. 123 (2001) 9597.
[40] K.L. Yeung, S.T. Yau, A.J. Maira, J.M. Coronado, J. Soria, P.L. Yue, J. Catal. 219 (2003) 107.
[41] M. Primet, P. Pichat, M.-V. Mathieu, J. Phys. Chem. 75 (1971) 1216.
[42] M. Hermann, H.P. Boehm, Z. Anorg. Allg. Chem. 368 (1969) 73.
[43] J.A. Navio, C. Cerrillos, C. Real, Surf. Interface Anal. 24 (1996) 355.
[44] G. Qi, R.T. Yang, J. Phys. Chem. B 108 (2004) 15738.
[45] X.Z. Fu, L.A. Clark, Q. Yang, M.A. Anderson, Environ. Sci. Technol. 30 (1996) 647.
[46] S.A. Larson, J.L. Falconer, Catal. Lett. 44 (1997) 57.
[47] X.B. Chen, C. Burda, J. Phys. Chem. B 108 (2004) 15446.